11. D. Schomburg, I. Schomburg, *Springer Handbook of Enzymes* (Springer, New York, ed. 2, 2001).
12. H. P. Lerch, A. S. Mikhailov, B. Hess, *Proc. Natl. Acad. Sci. U.S.A.* **99**, 15410 (2002).
13. T. E. Starr, N. L. Thompson, *Biophys. J.* **80**, 1575 (2001).
14. F. de Lange *et al.*, *J. Cell Sci.* **114**, 4153 (2001).
15. E. Betzig, R. J. Chichester, *Science* **262**, 1422 (1993).
16. D. R. Reyes, D. Iossifidis, P.-A. Auroux, A. Manz, *Anal. Chem.* **74**, 2623 (2002).
17. P.-A. Auroux, D. Iossifidis, D. R. Reyes, A. Manz, *Anal. Chem.* **74**, 2637 (2002).
18. H. G. Craighead, *Science* **290**, 1532 (2000).
19. J. D. Jackson, *Classical Electrodynamics* (Wiley & Sons, New York, ed. 3, 1999).
20. K. Rippe, *Biochemistry* **39**, 2131 (2000).
21. J. Ricka, T. Binkert, *Phys. Rev. A* **39**, 2646 (1989).
22. Materials and methods are available as supporting material on *Science* Online.
23. D. Kleppner, *Phys. Rev. Lett.* **47**, 233 (1981).
24. E. M. Purcell, *Phys. Rev.* **69**, 681 (1946).
25. E. Yablonivitch, *Phys. Rev. Lett.* **58**, 2059 (1987).
26. C. Xu, W. W. Webb, in *Topics in Fluorescence Spectroscopy*, vol. 5, *Nonlinear and Two-Photon-Induced Fluorescence*, J. Lakowicz, Ed. (Plenum Press, New York, 1997), pp. 471–540.
27. E. L. Elson, D. Magde, *Biopolymers* **13**, 1 (1974).
28. N. L. Thompson, T. P. Burghardt, D. Axelrod, *Biophys. J.* **33**, 435 (1981).
29. D. E. Koppel, *Phys. Rev. A* **10**, 1938 (1974).
30. Coumarin-dCTP was found to be efficiently and processively incorporated into DNA by Sequenase (USB Corporation, Cleveland, OH), a mutant T7 DNA polymerase. Detailed reaction conditions are given in (*22*).
31. S. S. Patel, I. Wong, K. A. Johnson, *Biochemistry* **30**, 511 (1991).
32. J. Korlach *et al.*, Patent Cooperation Treaty International Application No. WO 0070073, Cornell Research Foundation (2000).

33. We thank K. Hodgson for Fig. 1, M. Isaacson for obtaining Fig. 3D, and Amersham Biosciences for providing R110-dCTP. Supported by grant DE-FG02-99ER62809 from the U.S. Department of Energy. Additional support was received from NSF grant DBI-0080792 and from the facilities of National Center for Research Resources –NIH Biomedical Technology Resource, grant P41-RR04224, and the Nanobiotechnology Center, NSF–Science and Technology Center grant agreement ECS-9876771. Device fabrication was performed at the Cornell Nanofabrication Facility.

Supporting Online Material

www.sciencemag.org/cgi/content/full/299/5607/682/DC1
Materials and Methods
SOM Text
Figs. S1 and S2
Movies S1 and S2

23 October 2002; accepted 12 December 2002

Nitriding Iron at Lower Temperatures

W. P. Tong,[1] N. R. Tao,[1] Z. B. Wang,[1] J. Lu,[2] K. Lu[1]*

The microstructure in the surface layer of a pure iron plate was refined at the nanometer scale by means of a surface mechanical attrition treatment that generates repetitive severe plastic deformation of the surface layer. The subsequent nitriding kinetics of the treated iron with the nanostructured surface layer were greatly enhanced, so that the nitriding temperature could be as low as 300°C, which is much lower than conventional nitriding temperatures (above 500°C). This enhanced processing method demonstrates the technological significance of nanomaterials in improving traditional processing techniques and provides a new approach for selective surface reactions in solids.

Most surface-modification techniques used for solid materials are based on various chemical reactions that produce optimized structure and properties in order to improve the global performance of the materials. However, widespread uses of these techniques are frequently hindered by the reaction kinetics involved. For example, nitriding is a chemical treatment widely used to form surface nitrides. This technique is of great industrial interest, because it forms a unique composite structure with a hard surface (a layer of Fe-nitride compounds) and a tough interior, so that the global mechanical performance and wear/corrosion resistance of alloys and steels can be greatly improved (*1*). However, nitriding processes are performed at high temperatures (>500°C) for a long duration (~20 to 80 hours) (*1*, *2*) and may induce serious deterioration of the substrate in many families of materials.

A change of the surface microstructure by means of grain refinement is one option that can be used to accelerate the chemical reaction of a material surface. It is known that nanocrystalline materials possess ultrafine grains with a large number of grain boundaries that may act as fast atomic diffusion channels (*3*, *4*). Greatly enhanced atomic diffusivities in nanocrystalline materials relative to their conventional coarse-grained counterparts have been experimentally observed (*5*, *6*). A large number of grain boundaries with various kinds of nonequilibrium defects also constitutes a high excess stored energy that may further facilitate their chemical reactivity. It has been demonstrated experimentally that chemical reaction (or phase transformation) kinetics are greatly enhanced during mechanical attrition of solids, in which the grain size is significantly reduced to the nanometer scale and structural defects are created by the severe plastic deformation (*7*–*9*). Nitriding of iron was observed when Fe powders were processed in situ by ball-milling in a nitrogen-containing atmosphere at nominal ambient temperature (*10*, *11*), although a considerable transient temperature rise (as high as a few hundred degrees) always accompanies the impacts of the milling balls and may have contributed to an enhanced chemical reactivity.

We demonstrate enhanced chemical reaction kinetics at lower temperatures when the surface layer of a metal is transformed into a nanocrystalline structure, using the nitriding of Fe as an example. Our experimental observations show that surface nanocrystallization greatly facilitates the nitriding process, and it thus provides an alternative approach to surface modification of metallic materials.

A surface layer with nanocrystalline grains can be produced on a bulk metal by using a recently developed surface mechanical attrition treatment (SMAT) (*12*–*14*). The basic principle of the treatment is the generation of plastic deformation in the top surface layer of a bulk material by means of repeated multidirectional impacts of flying balls on the sample surface (Fig. 1A). The plastic deformation in the surface layer with a large strain and a high strain rate results in a progressive refinement of coarse grains into the nanometer regime. Stainless steel balls (with a mirrorlike surface and a diameter of

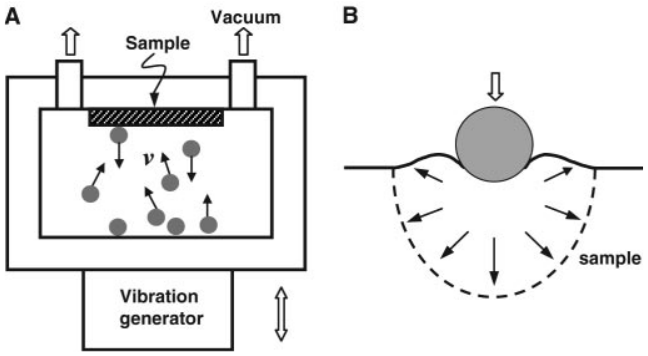

Fig. 1. Schematic illustrations of (**A**) the SMAT technique and (**B**) the localized plastic deformation zone induced by the vibrating ball.

[1]Shenyang National Laboratory for Materials Science, Institute of Metal Research, Chinese Academy of Sciences, Shenyang 110016, China. [2]Laboratoire des Systèmes Mécaniques et d'Ingénierie Simultanée (LASMIS), University of Technology of Troyes, 10000, Troyes, France.

*To whom correspondence should be addressed. E-mail: lu@imr.ac.cn

8 mm) were placed at the bottom of a cylinder-shaped vacuum chamber attached to a vibration generator. Because of the high vibration frequency of the system (50 Hz in this work), the sample surface under treatment was struck repetitively by a large number of balls within a short period of time, resulting in the sample surface becoming severely plastically deformed (Fig. 1B). As a consequence, grains in the surface layer (which could be as much as 50 μm thick) were effectively refined into the nanometer scale.

An iron plate (7 mm by 100 mm by 100 mm in size) with a purity of 99.95 weight percent (wt %) was treated to achieve a nanostructured surface layer. Before treatment, the Fe sample was annealed at 950°C for 120 min to eliminate the effect of mechanical polishing on the surface structure and to obtain homogeneous coarse grains of the α-Fe phase (~100 μm). The sample was protected by a high-purity argon atmosphere during the SMAT to avoid oxidation, and after treatment (a duration of 60 min) the sample surface was free of fractures and had mirrorlike smoothness (surface roughness was less than 1 μm), which is comparable to that of the original sample. Positron annihilation spectroscopy experiments indicated that the surface layer of the treated Fe sample was free of porosity. A detailed microstructural characterization of the nanostructured surface, together with a description of the underlying nanocrystallization mechanism during the SMAT in terms of the severe plastic deformation mode of bulk materials (*15*, *16*), can be found in (*17*).

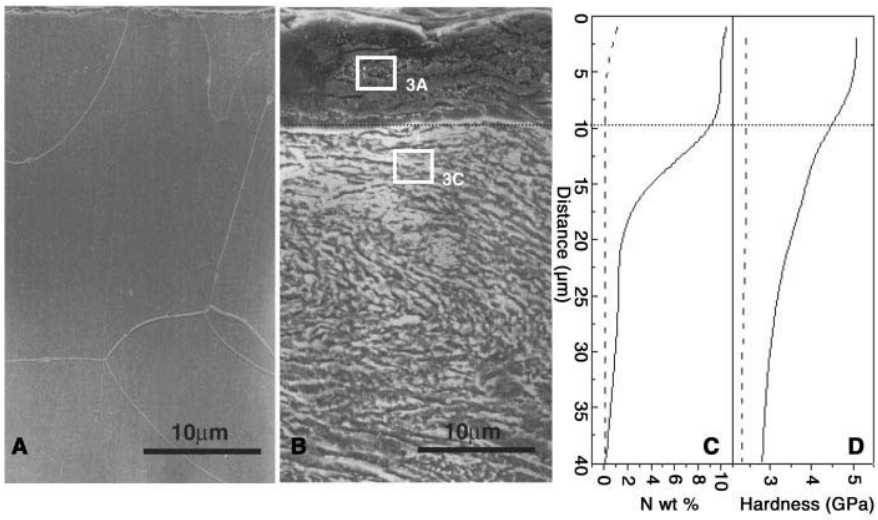

Fig. 2. Cross-sectional observations of (**A**) an original coarse-grained Fe sample and (**B**) a SMAT Fe sample after nitriding at 300°C for 9 hours. [In (B), 3A indicates Fig. 3A and 3C indicates Fig. 3C.] We measured (**C**) nitrogen concentration (by using an electron probe) and (**D**) microhardness (using nanoindentation) along the depth from the top surface layer in the original Fe sample (dashed lines) and in the treated one (solid lines), respectively.

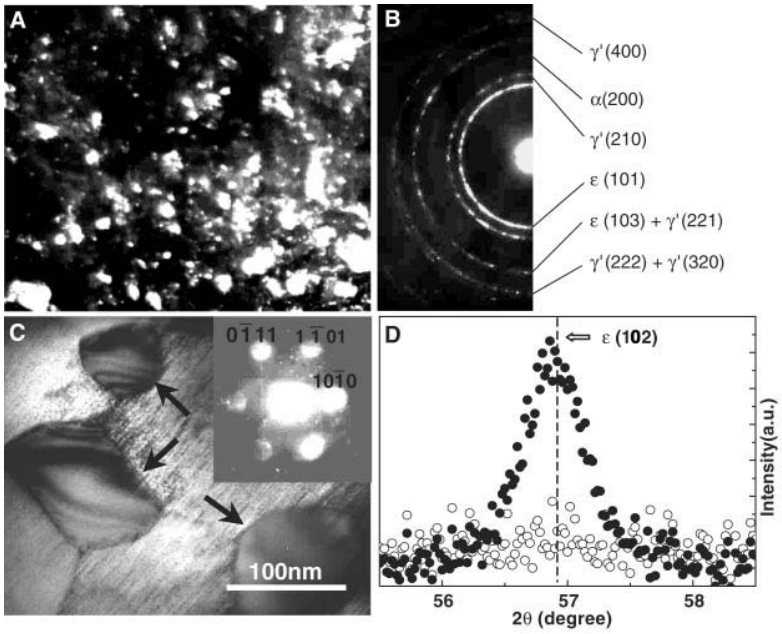

Fig. 3. (**A**) A dark-field TEM image and (**B**) the corresponding electron diffraction pattern for the compound layer indicated in Fig. 2B. (**C**) A TEM image for the microstructure beneath the compound layer indicated in Fig. 2B. Indicated by arrows are ε-phase particles, as confirmed by the electron diffraction pattern (inset) formed at grain boundaries and junctions of the α-Fe phase. (**D**) An XRD profile of the ε (102) peak for the SMAT Fe sample (solid circles) and the original sample (open circles) after nitriding at 300°C for 9 hours. The dashed line indicates the tabulated 2θ position for the ε (102) peak.

Both the untreated and treated samples were nitrided in flowing, high-purity ammonia gas (NH_3) at 300°C for 9 hours. Experiments showed that apparent grain growth of the nanocrystalline α-Fe phase in the surface layer may occur at 400°C or above, and the average grain size of the α-Fe nanophase was measured to be about 13 nm at 300°C after 9 hours, indicating a rather weak grain growth tendency at this temperature.

After nitriding, a continuous dark gray surface layer about 10 μm thick was observed on the SMAT Fe sample (Fig. 2B). This layer was not seen on the original (Fig. 2A). Measured nitrogen profiles (Fig. 2C) showed that nitrogen concentration was very high (about 10 wt %) in the dark gray layer, and it gradually dropped with increasing depth beneath the dark gray layer. In the original sample, the nitrogen concentration was negligible from the top surface to the substrate. Transmission electron microscope (TEM) observations, combined with electron diffraction, verified that the dark gray layer was composed of ultrafine polycrystalline ε-$Fe_{2\sim3}N$ and γ′-Fe_4N compounds, as well as a small amount of α-Fe phase (Fig. 3, A and B). The constitution was identical to that of the compound layer formed during the conventional nitriding of coarse-grained Fe at high temperatures. Underneath the compound layer was a mixture of nitrides and α-Fe solid solution (Fig. 3C). This evidence shows that the nitride (ε-$Fe_{2\sim3}N$) phase forms at the grain boundaries (or junctions) of the ultrafine-grained α-Fe phase. With increasing depth, the volume fraction of nitrides in the mixture layer decreases. X-ray diffraction (XRD) analysis confirmed the presence of iron nitrides (ε-$Fe_{2\sim3}N$ and γ′-Fe_4N) in the SMAT sample after nitriding (Fig. 3D), which differs from that in the original Fe sample, where no nitride was detected.

Nanoindentation measurements (made with a Nanoindenter XP, MTS Systems Corp., Eden Prairie, MN) indicated that the compound layer exhibited a much greater hardness [about 5.0 GPa, which is close to that for the conventional compound layer (*1*)] than the substrate (~2.3 GPa) (Fig. 2D). The variation of hardness along

depth agrees well with the structural and compositional analysis results. No hardness variation was noticed in the untreated sample after nitriding at this temperature. Tribological characterization of the samples after nitriding was performed by nanoindentation tests (standard nanoscratch tests) using a Berkovich diamond indenter with a tip radius of about 200 nm. The coefficients of friction and penetration curves for both samples were measured by scratching a total distance of 400 μm under a constant load of 400 mN. Results showed that the coefficient of friction of the treated sample, which was 0.38 ± 0.06 over the whole scratch length, was smaller than that of the original sample (0.52 ± 0.03) (which is close to that of the coarse-grained Fe without nitriding treatment) (fig. S1). Profiling of the scratch surface showed that the penetration depth on the nitrided SMAT Fe sample was less than 1 μm, whereas it was about 2.5 ± 0.5 μm for the untreated sample under the same load. The nanoscratch experiments were repeated several times with very consistent results, indicating enhanced wear and friction resistance of the surface layer after SMAT and nitriding.

Corrosion resistance of the nitrided Fe sample after SMAT was considerably increased relative to the original Fe sample, as indicated by the measured corrosion rate (current) as a function of immersion time for both samples with a polarization voltage of ±40 mV in a 3.5 wt % NaCl solution at ambient temperature (fig. S2). The corrosion current was about 0.11 ± 0.01 mA/cm^2 for the original Fe sample during the whole tested immersion time (120 hours), whereas it was only 0.03 ± 0.01 mA/cm^2 for the nitrided SMAT Fe sample with the compound surface layer. Once the compound layer was fully corroded after about 65 hours of immersion, the corrosion rate gradually increased and approached the value of the coarse-grained Fe sample.

The much-depressed nitriding temperature may be attributed to enhanced nitrogen diffusion in the nanocrystalline surface layer relative to the coarse grains. In conventional nitriding of coarse-grained iron, nitrogen diffusion in the Fe lattice dominates. In the nanocrystalline Fe sample, however, nitrogen mostly diffuses along Fe grain boundaries because of a much smaller activation energy (approximately half) compared with that for the lattice diffusion. Based on the literature data (*18*), nitrogen diffusivity in an α-Fe lattice is about 3.8×10^{-8} cm^2/s at 500°C, and it is about two orders of magnitude smaller (5.4×10^{-10} cm^2/s) at 300°C. Nitrogen diffusivity along grain boundaries at 300°C is estimated to be about 3.3×10^{-7} cm^2/s (based on an activation energy of about 0.6 times that for the lattice diffusion), which is three orders of magnitude larger than the lattice diffusion at the same temperature and is even higher than the nitrogen diffusivity in the lattice at 500°C. Evidently, the ultrafine-grained Fe phase in the surface layer provides a large number of defective grain boundaries (and other defects) that enhance the nitrogen diffusion.

From a thermodynamic point of view, the driving force for nitride formation is also enhanced when the Fe phase is nanostructured. The Gibbs free energy change for the formation of nitrides in coarse-grained Fe at 500°C is about –8.22 kJ/mol for the γ′ phase and –1.69 kJ/mol for the ε phase. Yet at 300°C, both values become positive, thus implying that these nitrides cannot form at this temperature. The mechanically induced nanostructures store a large excess energy in the grain boundaries and grain interior in the form of nonequilibrium defects (such as dislocations), which constitutes an extra driving force for the nitride formation process. The estimated stored energy in a ball-milled nanocrystalline Fe sample with 10 nm grain size is about 2.3 kJ/mol (*7*). With this stored excess energy, one may find from calculations that the Gibbs free energy change for the formation of nitrides in the nanocrystalline α-Fe phase at 300°C becomes negative (i.e., the formation of nitrides becomes possible). Our experimental evidence confirmed that the mechanically induced surface nanocrystallization of Fe created a considerable amount of stored energy in the surface layer that constitutes an effective driving force for the nitriding process at low temperatures.

Similarly, other surface chemical treatments that are controlled by the diffusion of foreign atoms (such as chromium or aluminum) and are used in industry to improve the performance of engineering materials can also be enhanced by SMAT. We found a greatly enhanced diffusivity of chromium in the SMAT Fe at 350°C, which is about 300° to 400°C lower than the conventional treatment temperature.

The substantial reduction of the nitriding temperature by means of surface nanocrystallization is a marked advancement for materials processing. The reduced nitriding temperature may allow for the nitriding of materials families (such as alloys and steels) and work-pieces that cannot be treated by conventional nitriding.

References and Notes

1. T. Bell, *Source Book on Nitriding* (American Society for Metals, Metals Park, OH, 1977).
2. J. Mongis, J. P. Peyre, C. Tournier, *Heat Treat. Metals* **3**, 71 (1984).
3. H. Gleiter, *Prog. Mater. Sci.* **33**, 223 (1989), and references therein.
4. K. Lu, *Mater. Sci. Eng. R Rep.* **16**, 161 (1996).
5. S. Schumacher, R. Birringer, R. Strauss, H. Gleiter, *Acta Metall.* **37**, 2485 (1989).
6. L. Lu, M. L. Sui, K. Lu, *Science* **287**, 1463 (2000).
7. H. J. Fecht, in *Nanophase Materials: Synthesis, Properties, Applications*, G. C. Hadjipanayis, R. W. Siegel, Eds. (Kluwer Academic, Dordrecht, Netherlands, 1994).
8. C. C. Koch, *Nanostruct. Mater.* **2**, 109 (1993).
9. C. Suryanarayana, *Prog. Mater. Sci.* **46**, 1 (2001).
10. A. Calka, J. I. Nikolov, J. S. Williams, *Mater. Sci. Forum*, **225–227**, 527 (1996).
11. M. S. El-Eskandarany, K. Sumiyama, K. Aoki, K. Suzuki, *Mater. Sci. Forum* **88–90**, 801 (1992).
12. K. Lu, J. Lu, *J. Mater. Sci. Technol.* **15**, 193 (1999).
13. _____, *Mater. Sci. Eng. A*, in press.
14. N. R. Tao, M. L. Sui, J. Lu, K. Lu, *Nanostruct. Mater.* **11**, 433 (1999).
15. N. Hansen, *Metall. Mater. Trans.* **32A**, 2917 (2001).
16. R. Z. Valiev, R. K. Islamgaliev, I. V. Alexandrov, *Prog. Mater. Sci.* **45**, 103 (2000).
17. N. R. Tao *et al.*, *Acta Mater.* **50**, 4603 (2002).
18. J. D. Fast, M. B. Verrijp, *J. Iron Steel Inst.* **176**, 24 (1954).
19. Supported by the Chinese National Science Foundation (grant 50021101), the Chinese Ministry of Science and Technology (grant G1999064505), the New Energy and Industrial Technology Development Organization (NEDO) International Joint Research Grant program (grant 01MB5), and the French Ministry of Research (grants 2001882 and CPER EN2040). We acknowledge critical reading of the manuscript by R. Yang and Z. H. Jin.

Supporting Online Material

www.sciencemag.org/cgi/content/full/299/5607/686/DC1
Figs. S1 and S2

6 November 2002; accepted 4 December 2002

Asynchronous Climate Changes in the North Atlantic and Japan During the Last Termination

Takeshi Nakagawa,[1]* Hiroyuki Kitagawa,[2] Yoshinori Yasuda,[1] Pavel E. Tarasov,[3] Kotoba Nishida,[4] Katsuya Gotanda,[1] Yuki Sawai,[1] Yangtze River Civilization Program Members[1]

Pollen records from the annually laminated sediment sequence in Lake Suigetsu, Japan, suggest a sequence of climate changes during the Last Termination that resembles that of the North Atlantic region but with noticeable differences in timing. An interstadial interval commenced a few centuries earlier [~15,000 years before the present (yr B.P.)] than the North Atlantic GI-1 (Bölling) event. Conversely, the onset of a Younger Dryas (YD)–like cold reversal (12,300 to 11,250 yr B.P.) postdated the North Atlantic GS-1 (YD) event by a few centuries. Climate in the Far East during the Last Termination reflected solar insolation changes as much as Atlantic influences.

One of the most pressing matters in late Quaternary paleoclimate research is to establish whether abrupt climatic events were globally synchronous, for this is pivotal to testing ideas about the mechanisms of global climate change. The main obstacle to